Adsorption of Acetone Both on the Clean Ru(001) Surface and on the Ru(001) Surface Modified Chemically by the Presence of an Ordered Oxygen Adatom Overlayer

A. B. Anton, N. R. Avery,† B. H. Toby, and W. H. Weinberg*

Contribution from the Division of Chemistry and Chemical Engineering, California Institute of Technology, Pasadena, California 91125. *Received August 23, 1985*

Abstract: The adsorption of acetone on the clean Ru(001) surface and the Ru(001) surface on which an ordered p(2 × 2) overlayer of oxygen adatoms is present has been investigated via electron energy loss vibrational spectroscopy and thermal desorption mass spectrometry. On both surfaces, two fundamentally different forms of adsorbed acetone coexist at temperatures below approximately 200 K—an η^1 species, bonded end-on through the oxygen atom, and an η^2 species, bonded side-on through both the oxygen atom and the acyl carbon atom. Both of these types of bonding have been identified previously in homogeneous organometallic complexes. On the clean Ru(001) surface, the η^2 species is dominant, with the η^1 species present only in low concentrations. Addition of the p(2 × 2)O overlayer increases the Lewis acidity of the Ru(001) surface, stabilizing η^1-acetone with respect to η^2-acetone. The η^1 species desorbs molecularly upon heating of the surface, whereas the more strongly bound η^2 species is an intermediate to dissociation. The results are compared with acetone adsorption on the Pt(111) surface and to the chemistry of analogous organometallic coordination complexes. The nature of the bonding on the two Ru(001) surfaces is interpreted in terms of the electronic structures of both the ketonic ligand and the metallic substrate.

I. Introduction

One of the principal aims of organometallic chemistry is to provide an interpretive framework in which the mechanistic details of metal-catalyzed reactions can be understood.[1] Reactions are conducted under carefully controlled conditions, and all reactants and products are thoroughly characterized with regard to their structural and chemical properties, both by spectroscopic techniques and by comparison to theoretical descriptions of the metal–ligand bonding interactions which govern their behavior. The stable coordination geometries for reactants, intermediates, and products represent local minima on the potential energy surface which describes all the possible metal–ligand interactions for the particular system investigated, and both transition-state structures and microscopic reaction mechanisms can often be inferred without ambiguity by this procedure. Our present understanding of metal-assisted chemical reactions in solution is a tribute to, and a direct result of, the success of this type of analysis.

One of the obvious goals of modern surface science research is to extend these results to the understanding of analogous reactions which occur under heterogeneous conditions, catalyzed by (extended) metal surfaces. A similar procedure must be followed, including careful control of reaction conditions and thorough characterization of the metal surface on which the reactions occur. Again, the structures of adsorbed (i.e., coordinated) intermediates can be used to delimit the transition-state structure(s) and microscopic mechanism(s) which describe the surface reaction(s) observed. Within this context, it is clear that heterogeneous catalysis is in fact the organometallic chemistry of extended metal surfaces, and as one might expect, results obtained for metal–ligand interactions in homogeneous systems prove to be very valuable in the interpretation of results obtained on metal surfaces.

The success of this approach for both homogeneous and heterogeneous systems relies on the ability to determine experimentally the structures of coordinated reaction intermediates. In homogeneous studies, stable products can often be separated, purified, and crystallized, allowing detailed deduction of chemical bond lengths and bond angles via X-ray crystallography.[2] The surface-sensitive analogue, low-energy electron diffraction (LEED),[3] can be applied most easily to systems where a single reaction intermediate is formed in a translationally periodic, two-dimensional lattice on a single-crystalline metal surface.[4] Even on single-crystalline metal surfaces, more than one intermediate is frequently formed with no long-range order to facilitate a LEED analysis. Thus, other approaches must be taken to identify surface structures. Of the various spectroscopic techniques available presently for the identification of reaction intermediates on surfaces, both the sensitivity and the wide spectral range of high-resolution electron energy loss vibrational spectroscopy (EELS) make it arguably the most powerful tool for chemical analysis of adsorbed species on well-characterized surfaces of low area.[5] Although the structural information provided by vibrational spectroscopy does not directly measure bond lengths and bond angles, it does identify both the nature of the bond and the bond order, and through application of the selection rules appropriate to EELS on metal surfaces,[6] the chemical identity and orientation of adsorbed species can be determined. With this type of information at hand, a rigorous comparison of the chemistry of extended metal surfaces to that of corresponding organometallic complexes can be made.

This paper reports results obtained via EELS and thermal desorption mass spectrometry for the interaction of acetone with the clean Ru(001) surface and the Ru(001) surface on which there is an ordered p(2 × 2) overlayer of oxygen adatoms.[7] The results help to quantify the relationship between the Lewis acidity of a metal surface and its selectivity toward both reactive and nonreactive bonding configurations of adsorbed acetone, providing an enlightening comparison of the chemistry of these surfaces to the chemistry of analogous organometallic complexes.[8]

The interaction of acetone and similar substituted ketones, R_1R_2CO, with metal centers in homogeneous systems has been

† Current address: Division of Materials Science, C.S.I.R.O., Catalysis and Surface Science Laboratory, University of Melbourne, Parkville 3052, Victoria, Australia.

(1) See, for example: Collman, J. P.; Hegedus, L. S. "Principles and Applications of Organotransition Metal Chemistry"; University Science: Mill Valley, 1980.
(2) Wells. A. F. "Structural Inorganic Chemistry", 4th ed., Clarendon Press: Oxford, 1975.
(3) Pendry, J. P. "Low Energy Electron Diffraction"; Academic Press: London, 1974.
(4) One notable example is the successful determination via LEED of the structure of the ethylidyne species which ethylene and acetylene form upon reaction with the Pt(111) surface. See: Kesmodel, L. L.; Dubois, L. H.; Somorjai, G. A. *J. Chem. Phys.* **1979**, *70*, 2180. Steininger, H.; Ibach, H.; Lehwald, S. *Surface Sci.* **1982**, *117*, 685.
(5) Ibach, H.; Mills, D. L. "Electron Energy Loss Spectroscopy and Surface Vibrations"; Academic Press: New York, 1982; Chapter 6.
(6) Reference 5, Chapter 3.
(7) Rahman, T. S.; Anton, A. B.; Avery, N. R.; Weinberg, W. H. *Phys. Rev. Lett.* **1983**, *51*, 1979.
(8) Avery, N. R.; Weinberg, W. H.; Anton, A. B.; Toby, B. H. *Phys. Rev. Lett.* **1983**, *51*, 682.

0002-7863/86/1508-0684$01.50/0

the subject of a number of investigations. Two general classes of bonding configurations have been identified, characterized structurally, and correlated with the electronic properties of both of the (R_1 and R_2) substituents of the ketonic ligands and the metal centers to which they bond. Electron-deficient metals (those in high formal oxidation states, for example) and weakly electronegative substituents (such as the CH_3 groups of acetone) generally facilitate bonding via σ donation from the ligand to the metal to produce an η^1(O) configuration (bonded end-on to the metal through the oxygen atom and hereafter referred to as η^1).[9-12] In this case, the metal serves as a weak Lewis acid and accepts an electron pair from the ketonic ligand. For metals weakly basic in the Lewis sense, i.e., those in a low formal oxidation state, or for ketonic ligands with more electronegative substituents (R_1 and R_2 = H, CF_3, and Ph), an η^2(O,C) configuration (bonded side-on to the metal through both the carbon and oxygen atoms and hereafter referred to as η^2) occurs.[13-20] This type of interaction, first described by Dewar and by Chatt and Duncanson,[21] results from simultaneous donation of electrons from the π orbital of the ligand to the d orbitals of the metal and backdonation of metal d electrons to the π^*-antibonding orbital of the ligand. This is a general feature of the interaction of many unsaturated ligands with metals.[22-24] The understanding of conditions prevailing at metal surfaces which yield selectively these two types of coordination interactions is an important and worthwhile pursuit. For example, η^1-carbonyl ligands are quite labile and nonreactive, exchanging easily in solution with other more tightly bound ligands,[10] whereas η^2 bonding is postulated to be important in the formation of reactive intermediates in heterogeneously catalyzed reactions such as the Fischer–Tropsch synthesis.[25]

Although several investigations of acetone adsorption on metal surfaces have appeared in the literature,[26,27] only one report has presented an unequivocal determination of the binding configurations of acetone on a single-crystalline metal surface.[27] In this case of acetone adsorption on the clean Pt(111) surface, EELS and thermal desorption mass spectrometry were used to identify an η^1 species which desorbed reversibly and a small concentration of an η^2 species, some of which decomposed upon heating the crystal. These results provide a particularly useful contrast and comparison to the results reported here for the adsorption of acetone on the Ru(001) and Ru(001)-p(2 × 2)O surfaces.

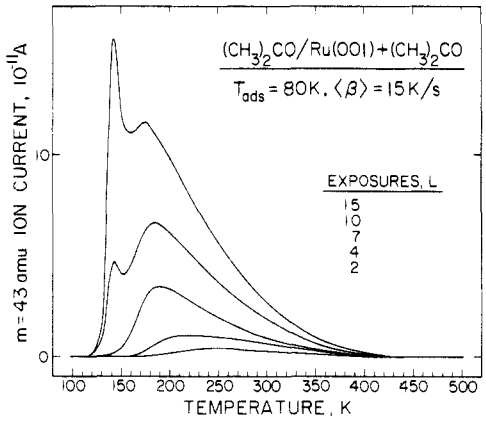

Figure 1. Thermal desorption spectra for increasing exposures of $(CH_3)_2CO$ on the clean Ru(001) surface at 80 K. The most abundant cracking fragment of $(CH_3)_2CO$, m = 43 amu, was monitored, and the average heating rate $\langle\beta\rangle$ was 15 K/s.

II. Experimental Procedures

A description of the EEL spectrometer and the ultrahigh vacuum (UHV) system in which it is contained has been published previously.[28] EEL spectra were recorded at a resolution of approximately 80 cm^{-1} (full-width at half-maximum) with a maximum count rate of 10^5 Hz in the specularly reflected, elastically scattered electron beam. Beam kinetic energies at the sample were between approximately 5 and 6 eV.

The Ru(001) surface was cleaned by thermal cycling between 400 and 1100 K in 10^{-7} torr of oxygen to remove surface impurities, followed by reductive annealing in vacuum at 1750 K.[29] Occasional Ar^+ sputtering was also used to clean the surface. Surface cleanliness was monitored via EELS and thermal desorption mass spectrometry, the surface was judged clean when the EEL spectrum was featureless, and the peak positions and intensities in thermal desorption spectra for various coverages of CO were reproduced. The ordered p(2 × 2) overlayer of oxygen adatoms, with an ideal surface coverage of 0.25 monolayer, was prepared by exposing the clean surface to 0.8 L of oxygen (1 L = 10^{-6} torr-s) at 95 K, followed by thermal ordering at a temperature of approximately 350 K.[7,30]

The $(CH_3)_2CO$ and $(CD_3)_2CO$ used in the experiments were degassed with multiple freeze–pump–thaw cycles, and their purities were verified in situ via mass spectrometry. The isotopically labeled compounds, $^{18}O_2$ and $(CD_3)_2CO$, were >99% purity in their specified isotopes. The crystal was exposed to all gases by backfilling the UHV chamber through leak valves, and exposures quoted in the text were measured with a Bayard-Alpert ionization gauge uncorrected for relative ionization cross sections.

Thermal desorption measurements were made in a line-of-sight mode with a UTI 100C quadrupole mass spectrometer, oriented approximately 40° from the surface normal. Surface coverages of hydrogen and CO reported for the (reaction product) thermal desorption measurements were obtained by comparing the time-integrated ion current for the desorption spectra to those obtained for desorption of known coverages of hydrogen[31] and CO.[32] The accuracy in this comparison is approximately ±10%.

Since the adsorbed overlayers were prepared by backfilling the UHV chamber, exposing uniformly all cold surfaces in the chamber to the particular adsorbate, and since the mass spectrometer had no provision for selective sampling of the single-crystalline surface, the features in the thermal desorption spectra associated with desorption from the crystal surface were superposed on a broad background signal due to desorption from all other chilled surfaces which are warmed during the collection of a thermal desorption trace. This is a particularly important consideration for a species such as acetone which condenses in UHV at liquid nitrogen temperatures. In the apparatus used for the experiments reported here, the Ru(001) sample was supported by two 0.020 in. diameter tantalum wires which were spot-welded to its rear face and clamped by two 0.109 in. diameter copper wires to form an electrical current path through the sample. The copper wires were in contact with a liquid nitrogen reservoir to provide conductive cooling of the sample, and

(9) Driessen, W. L.; Groeneveld, L. *Recl. Trav. Chim. Phys-Bas* **1969**, *88*, 977.
(10) Thompson, S. J.; White, C.; Maitlis, P. M. *J. Organomet. Chem.* **1977**, *136*, 87.
(11) Gould, R. O.; Sime, W. J.; Stephenson, T. A. *J. Chem. Soc. Dalton Trans.* **1978**, 76.
(12) Bennett, M. A.; Matheson, T. W.; Robertson, G. B.; Steffen, W. L.; Turney, T. W. *J. Chem. Soc., Chem. Commun.* **1979**, 32.
(13) Brown, K. L.; Clark, G. R.; Headford, C. E. L.; Marsden, K.; Roper, W. R. *J. Am. Chem. Soc.* **1979**, *101*, 503.
(14) Berke, H.; Bankhardt, W.; Huttner, G.; Seyerl, J. V.; Zsolnai, L. *Chem. Ber.* **1981**, *114*, 2754.
(15) Clarke, B.; Green, M.; Osborn, R. B. L.; Stone, F. G. A. *J. Chem. Soc. A* **1968**, 167.
(16) Browning, J.; Cundy, C. S.; Green, M.; Stone, F. G. A. *J. Chem. Soc. A* **1969**, 20.
(17) Countryman, R.; Penfold, B. R. *J. Cryst. Mol. Struct.* **1972**, *2*, 281.
(18) Wood, C. D.; Schrock, R. R. *J. Am. Chem. Soc.* **1979**, *101*, 5421.
(19) Green, M.; Howard, J. A. K.; Laguna, A.; Smart, L. E.; Spencer, J. L.; Stone, F. G. A. *J. Chem. Soc. Dalton Trans.* **1977**, 278.
(20) Adams, H.; Bailey, N. A.; Gauntlett, J. T.; Winter, M. J. *J. Chem. Soc., Chem. Commun.* **1984**, 1360.
(21) Dewar, M. J. S. *Bull. Soc. Chim. Fr.* **1951**, *18*, C79. Chatt, J.; Duncanson, L. A. *J. Chem. Soc.* **1953**, 2939.
(22) Greaves, E. O.; Lock, C. J. L.; Maitlis, P. M. *Can. J. Chem.* **1968**, *46*, 3879.
(23) Chisholm, M. H.; Clark, H. C. *Acc. Chem. Res.* **1973**, *6*, 202.
(24) Ittel, S. D. *Inorg. Chem.* **1977**, *16*, 2589.
(25) Henrici-Olivé, G.; Olivé, S. *Angew. Chem., Int. Ed. Engl.* **1976**, *15*, 136 and references therein.
(26) Blyholder, G.; Neff, L. D. *J. Phys. Chem.* **1966**, *70*, 893. Young, R. P.; Sheppard, N. *J. Catal.* **1967**, *7*, 223. Blyholder, G.; Shihabi, D. *J. Catal.* **1977**, *46*, 91. Lüth, H.; Rubloff, G. W.; Grobman, W. D. *Surface Sci.* **1977**, *63*, 325.
(27) Avery, N. R. *Surface Sci.* **1983**, *125*, 771.
(28) Thomas, G. E.; Weinberg, W. H. *Rev. Sci. Instrum.* **1979**, *50*, 497.
(29) Thomas, G. E.; Weinberg, W. H. *J. Chem. Phys.* **1979**, *70*, 954.
(30) Madey, T. E.; Engelhardt, H. A.; Menzel, D. *Surface Sci.* **1975**, *48*, 304.
(31) Shimizu, H.; Christmann, K.; Ertl, G. *J. Catal.* **1980**, *61*, 412.
(32) Williams, E. D.; Weinberg, W. H. *Surface Sci.* **1979**, *82*, 93.

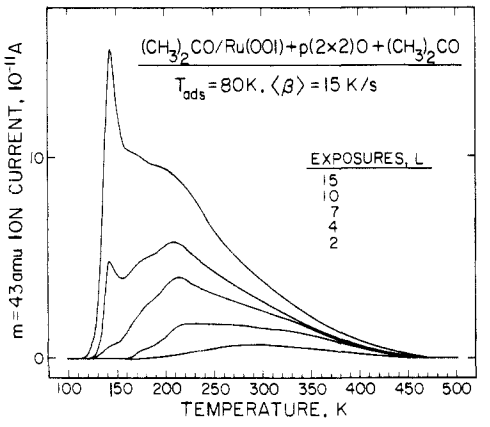

Figure 2. Thermal desorption spectra recorded under conditions identical with those of Figure 1 except for adsorption on the Ru(001)-p(2 × 2)O surface.

heating was accomplished by conduction of the heat generated almost totally by the tantalum wires to the sample as an electric current was passed through the sample via the copper and tantalum support leads. The heavy copper leads were also warmed by conduction of heat from the tantalum support wires, but their temperature lagged well behind that of the Ru(001) sample. The net result of these effects, then, for a thermal desorption spectrum of the mass spectrometer signal intensity vs. sample temperature for acetone desorption was to yield first a small, narrow signal burst at the beginning of the temperature ramp due to desorption from the rapidly heated tantalum leads and then features at their characteristic temperatures for desorption from the Ru(001) surface, superposed on a broad, slowly varying background due to desorption of condensed acetone from the slowly warming copper leads. For rather sharp desorption features, as were observed in the thermal desorption spectra for the H_2 and CO decomposition products, the background base lines in the spectra can be identified unambiguously, and the contribution due to desorption from the Ru(001) surface can be separated clearly. For broad features, however, as were observed for the desorption of molecular acetone from both the clean Ru(001) and the Ru(001)-p(2 × 2)O surfaces, the base lines were less certain. In all thermal desorption spectra presented below, the sharp burst at low temperatures and best estimates of the base lines due to background desorption have been subtracted for a more useful illustration of the experimental results. For the molecular acetone desorption spectra of Figures 1 and 2, however, the uncertainty in the amplitudes of the broad feature which extends from approximately 200–450 K prevents a quantitative determination of the total amounts of acetone desorption in the spectra. The qualitative differences in the spectra, to be discussed later, namely the increased amount of molecular desorption from the Ru(001)-p(2 × 2)O surface for a given acetone exposure as compared to the clean surface, are reliable and are the most noteworthy results evident in Figures 1 and 2.

III. Results

A. Thermal Desorption Spectra of Acetone from the Clean Ru(001) and the Ru(001)-p(2 × 2)O Surfaces. Thermal desorption spectra recorded after the indicated exposures of the clean Ru(001) surface to $(CH_3)_2CO$ at 80 K are shown in Figure 1. For exposures below 4 L, almost no molecular acetone desorption is observed. For exposures of 4 L and above, however, a broad feature with a desorption rate maximum near 220 K, shifting with increasing exposure to 180 K for a monolayer saturation exposure, is observed. A peak due to the formation of a condensed multilayer appears at 140–150 K for exposures greater than 7 L. This multilayer state first appears at exposures below that necessary to saturate the monolayer state, suggesting that some "clustering" may occur, as has been observed in the thermal desorption spectra of H_2O from the Ru(001) surface.[33] No evidence for a "second layer" desorption state, like that observed for acetone adsorption on Pt(111),[27] can be extracted unambiguously from the thermal desorption spectra of Figure 1, although some evidence for such a state is observed in the EELS results to be presented below.

Noteworthy is the "tailing" of the monolayer desorption feature from its desorption rate maximum near 200 K to approximately

(33) Thiel, P. A.; Hoffmann, F. M.; Weinberg, W. H. *J. Chem. Phys.* **1981**, *75*, 5556.

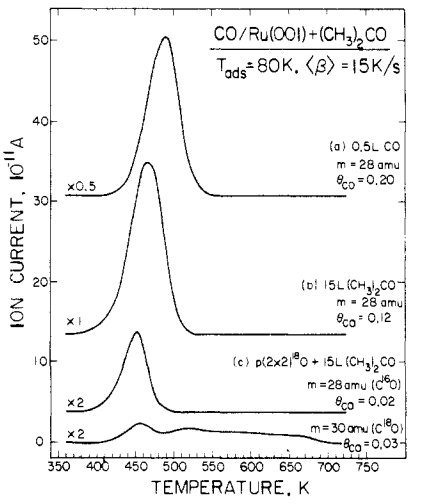

Figure 3. Thermal desorption spectra for the CO decomposition product from 15-L exposures of the clean Ru(001) and the Ru(001)-p(2 × 2)^{18}O surfaces to $(CH_3)_2CO$. The top spectrum shows CO desorption following exposure of the clean surface to 0.5 L of CO for comparison.

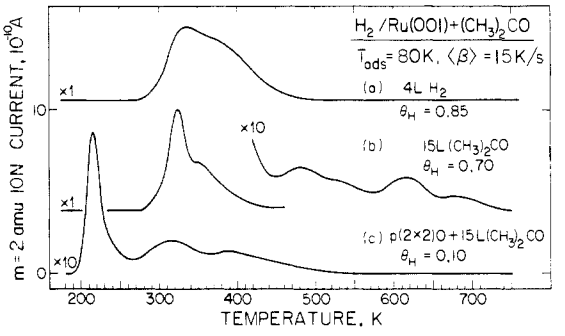

Figure 4. Thermal desorption spectra for the H_2 decomposition products from 15-L exposures of the clean Ru(001) and the Ru(001)-p(2 × 2)O surfaces to $(CH_3)_2CO$. The top spectrum shows H_2 desorption following exposure of the clean surface to 4 L of H_2 for comparison.

400 K. This indicates a broad range of binding energies for the monolayer molecular species, due perhaps to repulsive interactions which lower its binding energy at high coverages and are relieved as desorption progresses, or to attractive interactions of acetone with surface species present at higher temperatures (and lower surface coverages).

A series of thermal desorption spectra for exposures equal to those of Figure 1, but instead on the Ru(001)-p(2 × 2)O surface, are shown in Figure 2. Although qualitatively similar, several quantitative differences are apparent: more molecular acetone is evolved in the temperature range between 200 and 450 K for all exposures; two rate maxima for monolayer desorption, near 180 and 200 K, are observed; and the multilayer feature is clearly evident for lower exposures, appearing first at 7 L.

B. Thermal Desorption Spectra of the Decomposition Products, CO and H_2, from the Clean Ru(001) and the Ru(001)-p(2 × 2)O Surfaces. Hydrogen and CO are the only products of the decomposition of $(CH_3)_2CO$ on the clean and the Ru(001)-p(2 × 2)O surfaces, as detected by thermal desorption spectra. The desorption spectra recorded for these products are shown in Figures 3 and 4 following multilayer exposures (15 L) of both surfaces to $(CH_3)_2CO$ at 80 K. For comparison, spectrum a of Figure 3 shows desorption of CO from the clean Ru(001) surface following exposure to 0.5 L of CO (θ_{CO} adsorbed CO molecules per ruthenium surface atom = 0.20), and spectrum a of Figure 4 shows desorption of H_2 from the clean Ru(001) surface following exposure to 4 L of H_2 (θ_H = 0.85). For spectra c of both Figures 3 and 4, p(2 × 2)O overlayers were produced via adsorption of $^{18}O_2$ to allow separate detection of the CO produced by the decomposition of adsorbed $(CH_3)_2CO$, appearing at m = 28 amu, and that produced by reaction of adsorbed carbon from CH_3 decomposition, with the ^{18}O of the p(2 × 2)O overlayer appearing

at $m = 30$ amu. Furthermore, this increases the sensitivity of the thermal desorption measurement to H_2O ($m = 20$ amu), which might be expected to be a product of the reaction of $(CH_3)_2CO$ with the Ru(001)–p(2 × 2)O surface. However, no $H_2{}^{18}O$ was detected under any circumstances.

The CO evolution from a saturated monolayer of $(CH_3)_2CO$ on the clean Ru(001) surface, shown in Figure 3b, yields $\theta_{CO} = 0.12$, and since no CO_2, H_2O, or other oxygen-containing desorption products were observed, this demonstrates that the clean surface is active for the decomposition of approximately one-eighth of a monolayer of adsorbed acetone. This is to be compared with the $m = 28$ amu spectrum below it for the same exposure on the Ru(001)–p(2 × 2)O surface, Figure 3c, where $\theta_{CO} = 0.02$. Obviously, the presence of the ordered oxygen overlayer decreases the decomposition activity of the Ru(001) surface by a factor of approximately 6.

Proper stoichiometry in the overall surface decomposition reaction,

$$(CH_3)_2CO + 2{}^{18}O \rightarrow CO + 3H_2 + 2C{}^{18}O$$

would suggest that $\theta_{C^{18}O}$ for the $m = 30$ amu desorption spectrum of Figure 3d should be equal to 0.04 rather than 0.03. This discrepancy may be a result of an inaccurate base-line determination in the spectra, or more likely is due to slight ($\theta_{CO} = 0.05$) adsorption of background CO ($m = 28$ amu) from the chamber ambient during exposure to $(CH_3)_2CO$, making θ_{CO} for the associated $m = 28$ amu spectrum (Figure 3c) larger than the value of 0.015 necessary by stoichiometry to match the $\theta_{C^{18}O} = 0.03$ of the $m = 30$ amu spectrum.

The $m = 30$ amu desorption spectrum of Figure 3d identifies the temperature range over which adsorbed carbon and oxygen react to form and evolve CO, i.e., between approximately 400 and 700 K. The absence of CO desorption in this temperature range for the $m = 28$ amu spectra confirms that no carbon–oxygen bond cleavage occurs in the decomposition of adsorbed acetone.

The $m = 28$ amu desorption spectra of Figure 3b and c for the clean Ru(001) and the Ru(001)–p(2 × 2)O surfaces have the temperatures corresponding to their maximum desorption rates downshifted from 490 K, shown in the clean surface CO desorption spectrum of Figure 3a, to 470 and 455 K, respectively. This can be attributed to interactions between the adsorbed CO molecules and adsorbed hydrocarbon fragments[34] and the oxygen adatoms of the p(2 × 2)O overlayer.[35]

Comparison of the thermal desorption spectrum b of Figure 4, which shows H_2 evolution from a saturated monolayer of $(CH_3)_2CO$ on the clean Ru(001) surface, to that of Figure 4c for the same exposure on the Ru(001)–p(2 × 2)O surface shows an approximate sevenfold decrease in the amount of acetone decomposition upon the addition of the oxygen overlayer to the Ru(001) surface, a value that is consistent, within experimental uncertainties, with the results shown previously in Figure 3. Furthermore, the hydrogen coverages, obtained by comparison to the spectrum of Figure 4a for desorption from a saturation exposure of the clean surface to H_2, compare well with the values expected on the basis of the corresponding observed CO coverages and the stoichiometry expected from the aforementioned surface decomposition reaction, i.e., $\theta_H = 6\theta_{CO} = 0.72$ and 0.12, respectively.

The peak shapes of the thermal desorption spectra shown in Figure 4b and c are of particular interest. Comparison to results of thermal desorption measurements for coadsorbed overlayers of CO and hydrogen on Ru(001)[36] indicates that the H_2 desorption features appearing in Figure 4b between 280 and 450 K are due solely to the recombination of hydrogen adatoms on the Ru(001) surface in the presence of coadsorbed CO. The series of weak features between approximately 450 and 750 K are due to the decomposition of adsorbed hydrocarbon fragments which result from the decomposition of adsorbed acetone. In Figure 4c, the sharp feature at 220 K is due to hydrogen adatoms recombining in the presence of adsorbed oxygen, its shape and peak temperature depending sensitively on the presence of the p(2 × 2)O overlayer.[37] Features above 250 K in this spectrum, representing slightly more than half of the total yield of hydrogen from the surface, are due to the decomposition of adsorbed hydrocarbon fragments from acetone decomposition in this temperature range.

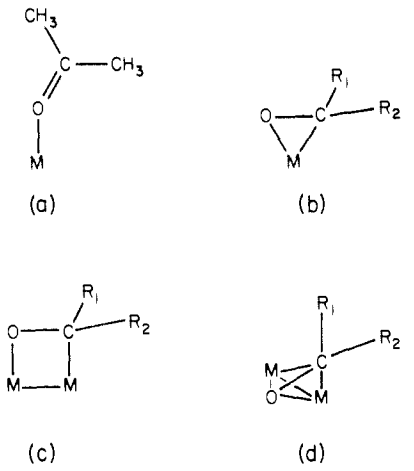

Figure 5. Schematic η^1 (a) and η^2 (b, c, and d) bonding configurations for ketonic ligands observed in homogeneous complexes.

Also noteworthy is the absence of H_2O production from the decomposition of $(CH_3)_2CO$ in the presence of the p(2 × 2)O overlayer. Although evidence for the reaction of disordered, adsorbed oxygen with hydrogen on Ru(001) to evolve H_2O has been obtained in the thermal decomposition of adsorbed HCOOH,[38] thermal desorption measurements recorded following hydrogen adsorption on the Ru(001)–p(2 × 2)O surface produce no H_2O, only desorption of H_2.[37] Thus, the relative probability of H_2O production vs. H_2 desorption depends sensitively on the long-range order of the oxygen overlayer. This can be explained by consideration of two important effects of the oxygen order on these reactions, both of which act to make hydrogen adatom recombination and desorption more likely. First, the formation of the ordered p(2 × 2)O overlayer upon the annealing of a disordered overlayer of adsorbed oxygen[7,30] indicates that attractive interactions which increase the Ru=O binding energy are maximized in the p(2 × 2) configuration, increasing the energy barrier to the abstraction of adsorbed oxygen by reaction with hydrogen. Second, the p(2 × 2)O overlayer destabilizes adsorbed hydrogen into a new binding state with an activation energy of desorption below 9 kcal/mol, desorbing near 220 K, as compared with the clean surface state, desorbing near 400 K with an activation energy of desorption of approximately 17 kcal/mol.[31]

C. EELS of Acetone on the Clean Ru(001) Surface. Exposures of the Ru(001) surface to 15 L or more of acetone at 95 K produces EEL spectra typical of the condensed species and virtually identical with the multilayer spectra reported for acetone adsorption on Pt(111).[27] The modes observed for multilayer $(CH_3)_2CO$ and their assignments based on a comparison with the IR and Raman spectra of liquid acetone[39] are listed in Table I.

The EEL spectra for the monolayer states of acetone both on the clean Ru(001) and the Ru(001)–p(2 × 2)O surfaces show evidence for species coordinated both in η^1 and η^2 configurations. Before attempting to assign the spectra, however, a review of the vibrational structure expected for both of these species will be helpful.

Consideration of the σ-bonding interaction which leads to coordination in an η^1 configuration, to be discussed later, indicates

(34) Hills, M. M.; Weinberg, W. H., unpublished results.
(35) Lee, H.-I.; Praline. G.; White, J. M. *Surface Sci.* **1980**, *91*, 581.
(36) Peebles, D. E.; Schreifels, J. A.; White, J. M. *Surface Sci.* **1982**, *116*, 117.
(37) Anton, A. B.; Weinberg, W. H., unpublished results.
(38) Avery, N. R.; Toby, B. H.; Anton, A. B.; Weinberg, W. H. *Surface Sci.* **1982**, *122*, L574. Toby, B. H.; Avery, N. R.; Anton, A. B.; Weinberg, W. H. *J. Electron Spectrosc.* **1983**, *29*, 233.
(39) Dellepiane, G.; Overend, J. *Spectrochim. Acta* **1966**, *22*, 593. Allkins, J. R.; Lippincott, E. R. *Spectrochim. Acta* **1968**, *25A*, 761.

Table I. Assignments of Vibrational Bands (in cm^{-1}) Observed with High-Resolution Electron Energy Loss Spectroscopy of $(CH_3)_2CO$ and $(CD_3)_2CO$ on Ru(001) and Ru(001)-p(2 × 2)O. Also Listed Are the Raman and IR Bands of Liquid Acetone and Their Symmetry Types for the Free Acetone Molecule

				EELS—acetone on Ru(001)				
	liquid acetone[39]			$(CH_3)CO$			$(CD_3)_2CO$	
mode	symmetry (C_{2v})	$(CH_3)_2CO$	$(CD_3)_2CO$	multilayer	η^1 (95 K)	η^2 (275 K)	η^1 (95 K)	η^2 (275 K)
ν(CO)	A_1	1711 (vs)	1701 (vs)	1720	1690	1300	1665–1675	1275
ν_a(C–C–C)	B_1	1221 (vs)	1249 (vs)	1240			1260	
ν_s(C–C–C)	A_1	787 (w)	696 (m)		780–825		715–720	
δ(CO)	B_1	530 (m)	478 (s)	535	515–540[a]		495–505[a]	
δ(C–C–C)	A_1	493 (w)	410 (w)					
π(CO)	B_2	393 (w)	331 (w)			655		610
		3006 (s)	2257 (s)				2210–2240	
$\nu(CH_3)$		2967 (s)	2222 (s)	3030	2950–2995	2955		2220
		2922 (s)	2109 (s)				2070–2090	
		1430 (s)	1088 (s)					
$\delta(CH_3)$		1361 (vs)	1037 (vs)	1380	1395–1440	1370	1030–1045	1075
		1356 (w)	1006 (w)					
		1092 (m)			1050–1110	1170		880
$\omega(CH_3)$		1066 (m)	889 (m)	905		980	920	
		902 (m)			890–905			820

[a] Not resolved from the mode at 530 cm^{-1} due to oxygen adatoms of the p(2 × 2)O overlayer.

that little perturbation of the structure of the acetone skeleton from that of the free molecule is expected in the η^1 configuration, depicted in Figure 5a. This is manifest in the vibrational spectra of η^1-acetone complexes by a preservation of the polarizations and only a weak perturbation of the frequencies of the methyl and nearly all of the skeletal vibrations of free acetone.[27] The only strongly affected mode is the ν(CO), which is red-shifted from its free acetone value of 1711 cm^{-1} to near 1650 cm^{-1} in a range of organometallic complexes of the type $\{[(CH_3)_2CO]_6M\}^{2+}$,[9] to 1661[11] and 1665 cm^{-1} [12] in two η^1-acetone complexes of ruthenium, and to 1630 cm^{-1} for η^1-$(CH_3)_2CO$ adsorbed on the Pt(111) surface.[27] The presence of a carbonyl band in this frequency range and methyl vibrations at frequencies characteristic of free acetone in the EEL spectra identify unambiguously the presence of η^1-acetone. The appearance in the spectra of other unperturbed skeletal vibrations with polarizations well-defined with respect to the symmetry properties of the acetone skeleton—ν_a(CCC), ν_s(CCC), δ(CO), δ(CCC), and π(CO)—will depend on the orientation of the adsorbed acetone skeleton with respect to the surface plane through consideration of the "dipolar selection rules" for adsorbate vibrations.[40] Such considerations can be used to determine the symmetry of the η^1-surface complex.[27]

The vibrational spectrum expected for acetone coordinated in an η^2 configuration is not so well-defined. Several η^2 configurations have been identified in the homogeneous chemistry of ketonic-like ligands with the general formula R_1R_2CO, including rigid three-membered rings with single metal centers, as in Figure 5b (e.g., $R_1 = R_2 = H$, M = Os,[13] M = Fe;[14] $R_1 = R_2 = CF_3$, M = Pt,[15] M = Ni;[16,17] and $R_1 = R_2 = CH_3$, M = Ta[18]), a rigid four-membered ring with two metal centers, as in Figure 5c ($R_1 = R_2 = CF_3$ and $M_1 = M_2$ = Pt[19]), and a perpendicular bridge (μ-η^2) configuration where the carbon–oxygen bond of the ligand bisects the bond between the two metal atoms, as in Figure 5d (e.g., $R_1 = CH_3$, $R_2 = H$, and $M_1 = M_2$ = Mo[20]). Any of these configurations must be considered a possible product of the interaction of acetone with the Ru(001) surface. Those complexes which have been characterized by vibrational spectroscopy show bands ascribed to ν(CO) in the range 1017–1220 cm^{-1},[13,14,18] signifying in all cases a substantial lowering of the carbon–oxygen bond order of the free ligand from two to nearly one upon coordination and rehybridization of the ketonic carbon from sp^2 to nearly sp^3. Those complexes characterized by an X-ray structural analysis show C–O bond lengths between 1.32 and 1.59 Å and significant deviation of the R_1–C–R_2 plane and the C–O bond from the coplanar configurations of the free ligands.[13,17,19,20] This is indicative of the rehybridization of the ketonic carbon which occurs as a result of electron donation to the π^*_{CO}-antibonding orbital of the ligand in all these configurations. Consequently, an adsorbed η^2-acetone should display a C–O vibration that is red-shifted by several hundred wavenumbers from that of the η^1 species and skeletal vibrations that are consistent with the rehybridization of the ketonic carbon to nearly sp^3.

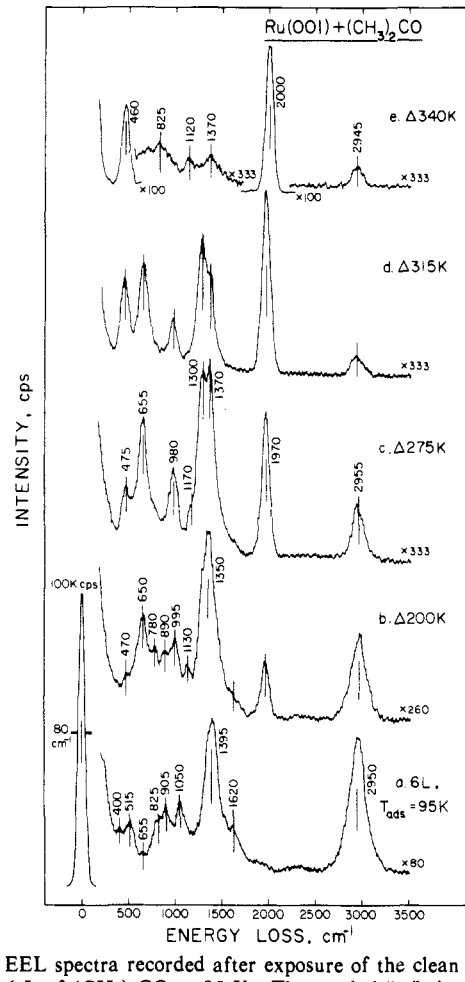

Figure 6. EEL spectra recorded after exposure of the clean Ru(001) surface to 6 L of $(CH_3)_2CO$ at 95 K. The symbol "Δ" signifies momentary heating to the indicated temperatures, followed by cooling to 95 K to record the spectra.

With this framework established, the results of the EELS experiments can now be interpreted. Figures 6 and 7 show EEL spectra recorded after exposure of the clean Ru(001) surface at 95 K to 6 L of $(CH_3)_2CO$ and 6 L of $(CD_3)_2CO$, respectively, followed by momentary annealing at the indicated temperatures and recooling to 95 K to record the spectra. Assignments of the

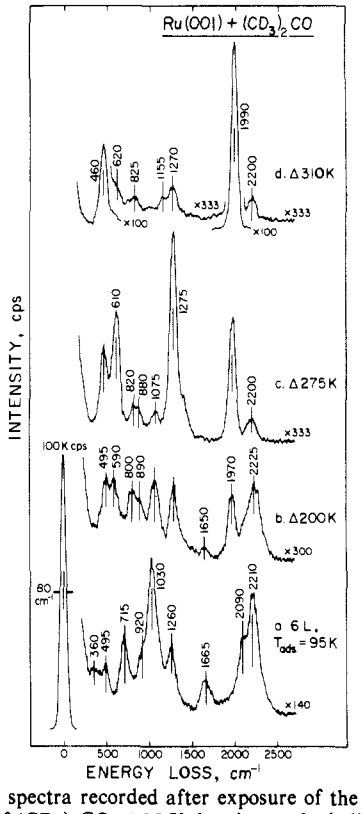

Figure 7. EEL spectra recorded after exposure of the clean Ru(001) surface to 6 L of $(CD_3)_2CO$ at 95 K, heating to the indicated temperatures, and recooling to 95 K.

surface species that are identified are listed in Table I.

Spectrum a of Figure 6, recorded immediately after adsorption at 95 K, shows strong modes at 2950, 1395, 1050, and 905 cm^{-1} due to the ν, δ, and ω modes of the CH_3 groups of adsorbed $(CH_3)_2CO$. The shoulder at 1620 cm^{-1}, its apparent position red-shifted somewhat from its true position by overlap with the tail of the strong $\delta(CH_3)$ band, signifies the existence of some $(CH_3)_2CO$ adsorbed in an η^1 configuration. The ν, δ, and ω modes of CH_3 appear with an intensity too great to be attributed solely to the η^1 species identified by ν(CO) at 1620 cm^{-1}, however, and must therefore result from the presence of another adsorbed species which coexists with η^1-$(CH_3)_2CO$ at this temperature and exposure. The appearance of clustering in the monolayer, as evidenced by the thermal desorption results discussed previously, and the identification of a "second-layer" state in the thermal desorption spectra for acetone adsorption on Pt(111)[27] suggest that the "extra" intensity in these features may be due to the onset of adsorption into the multilayer (or alternatively, a second layer) state at this exposure. A correspondingly strong feature due to the ν(CO) mode of A_1 symmetry of the multilayer species, expected at 1720 cm^{-1} (cf. Table I), is conspicuously absent, indicating via the dipolar selection rule that the molecules in this state are oriented with their molecular planes nearly parallel to the surface. This interpretation is substantiated by the presence of a weak mode at 400 cm^{-1}, which can be assigned most readily to the B_2 π(CO) vibration of the same second or multilayer species. The mode at 515 cm^{-1} and the poorly resolved feature labeled at 825 cm^{-1} are due to the B_1 δ(CO) and A_1 ν_s(CCC) vibrations of η^1-$(CH_3)_2CO$, respectively, and the feature at 655 cm^{-1} is the first indication of the presence of an η^2 species.

Annealing the surface to 200 K produces spectrum b of Figure 6. Substantial desorption has occurred (note the change of scale between spectra a and b), but a small amount of η^1-$(CH_3)_2CO$ remains, as evidenced by the presence of ν(CO) near 1620 cm^{-1}, $\omega(CH_3)$ at 890 cm^{-1}, and ν_s(CCC) at 780 cm^{-1}. New bands associated with η^2-$(CH_3)_2CO$ appear near 995 and 1130 cm^{-1}, the feature near 650 cm^{-1} gains intensity relative to the other modes in the spectra, and the broad band associated with $\delta(CH_3)$ shifts noticeably from 1395 to 1350 cm^{-1}. Some decomposition is evidenced by bands near 470 and 2000 cm^{-1} due to ν(RuC) and ν(CO) of the adsorbed CO.[29]

Before proceeding further with the $(CH_3)_2CO$ spectra, the corresponding behavior in the $(CD_3)_2CO$ spectra of Figure 7 should be addressed. The presence of η^1-$(CD_3)_2CO$ in spectrum a at 95 K is revealed by the ν(CO) mode at 1665 cm^{-1} and the A_1 ν_s(CCC) mode at 715 cm^{-1}. Again, the methyl vibrations—$\nu(CD_3)$ at 2210 and 2090 cm^{-1}, $\delta(CD_3)$ at 1030 cm^{-1}, and $\omega(CD_3)$ near 920 cm^{-1}—appear with anomalously high intensity compared to the ν(CO) mode at 1665 cm^{-1}, suggesting the presence of a second layer species, and the B_2 π(CO) of the latter is visible at 360 cm^{-1}. Other modes at 1260 and 495 cm^{-1} can be assigned to the B_1 ν_a(CCC) and B_1 δ(CO) modes of η^1-$(CD_3)_2CO$, respectively. Heating the surface to 200 K initiates decomposition, desorbs most of the η^1-$(CD_3)_2CO$, and reveals features due to η^2-$(CD_3)_2CO$ near 1260, 890, 800, and 590 cm^{-1}.

The EEL spectra of η^2-$(CH_3)_2CO$ and η^2-$(CD_3)_2CO$ are developed fully after annealing the surface to 275 K and are shown in Figures 6c and 7c, respectively, with assignments of these spectra listed in Table I. The band at 1300 cm^{-1} in the $(CH_3)_2CO$ spectrum, which is barely resolved from the $\delta(CH_3)$ band at 1370 cm^{-1}, and the band at 1275 cm^{-1} in the $(CD_3)_2CO$ spectrum are assigned to the ν(CO) mode of η^2-acetone, red-shifted by over 400 cm^{-1} from ν(CO) for free acetone and implying considerable skeletal reorganization in this bonding configuration. This significant rehybridization of the ketonic carbon atom from sp^2 toward sp^3, analogous to that observed in the η^2 complexes of related ligands described earlier, reduces the C–C–C bond angle of acetone toward a tetrahedral configuration, which is manifest in two other features of the η^2-acetone spectra. First, the $\omega(CH_3)$ modes typical of free and η^1-$(CH_3)_2CO$, expected near 900 and 1100 cm^{-1} (cf., Table I), are replaced by a strong band at 980 cm^{-1} and a weaker band at 1170 cm^{-1} in the spectrum of η^2-$(CH_3)_2CO$. This is a result of strong coupling between the methyl rocking modes and the C–C stretching mode of a CH_3 group bonded to an sp^3 carbon atom and is typical of isopropyl and *tert*-butyl configurations.[41] In isopropyl alcohol, for example, similar coupling leads to a strong band at 950 cm^{-1} and a weaker band at 1140 cm^{-1}.[42] As a result of this coupling, CH_3 rocking modes often do not yield good group frequencies, and the disparity between the frequencies of the coupled rocking modes in isopropyl alcohol and in η^2-$(CH_3)_2CO$ is of lesser significance than the fact that a strong band in the 900–1000 cm^{-1} region is expected for this type of structural configuration. In the spectrum of η^2-$(CD_3)_2CO$, the difference in frequency between the $\omega(CD_3)$ modes and the C–C stretching vibrations precludes strong coupling, and the $\omega(CD_3)$ modes appear with low intensity at 820 and 880 cm^{-1}, close to the values obtained for the corresponding vibrations of free $(CD_3)_2CO$. The second manifestation of the skeletal reorganization in η^2-acetone is the appearance of the band at 655 cm^{-1} for η^2-$(CH_3)_2CO$ and at 610 cm^{-1} for η^2-$(CD_3)_2CO$, which develops concomitantly with the other features ascribed to the η^2 species. This band is assigned to an O–C–C_2 angle bending vibration, which may be regarded as being derived from the weak π(CO) mode of free acetone at 393 cm^{-1} for $(CH_3)_2CO$ and 331 cm^{-1} for $(CD_3)_2CO$, respectively. With both the oxygen and carbon atoms of the carbonyl function bonded to the ruthenium surface in the η^2 configuration, this mode corresponds to the motion of the two methyls in unison up-and-down against the surface.

Further evidence justifying the assignment of bands near 655 and 1300 cm^{-1} in the η^2-acetone spectra to the signature skeletal vibrations can be obtained by consideration of the spectra shown in Figure 8. The bottom spectrum, recorded in the specular direction where dipolar inelastic scattering is dominant, is identical with that shown in Figure 6c. The top spectrum, recorded with the EELS analyzer rotated 6° toward the surface normal from the specular direction, is expected to show enhancement of features

(40) Reference 39, Chapter 4.
(41) Coltup, N. B.; Daly, L. H.; Wiberley, S. E. "Introduction to Infrared and Raman Spectroscopy"; Academic Press: New York, 1975; Chapter 5.
(42) Reference 41, p 458.

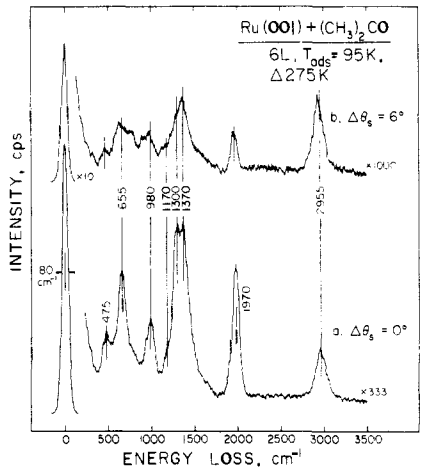

Figure 8. EEL spectra recorded in the specular direction (a) and 6° out of the specular direction (b), after exposure of the clean Ru(001) surface to 6 L of $(CH_3)_2CO$ at 95 K, heating to 275 K, and recooling to 95 K.

which include a significant contribution from (short-range) impact inelastic scattering relative to the (long-range) dipolar scattering. As has been shown previously, impact scattering is significant only for vibrational modes dominated by hydrogen or deuterium motion at the electron beam kinetic energy employed in these measurements.[6] Thus, the top spectrum of Figure 8 should show enhancement of the CH_3 modes relative to the skeletal modes. As may be seen, the ν(CO) and π(CO) modes at 1300 and 655 cm^{-1}, respectively, as well as the dipolar modes due to chemisorbed CO at 475 and 1970 cm^{-1}, have lost intensity relative to $\nu(CH_3)$ at 2955 cm^{-1}, $\delta(CH_3)$ at 1370 cm^{-1}, and $\omega(CH_3)$ at 1170 and 980 cm^{-1}, confirming the previous assignments and the correspondence indicated between the spectra for η^2-$(CH_3)_2CO$ and η^2-$(CD_3)_2CO$.

The dipolar selection rule for adsorbate vibrations indicates that only those vibrations which involve a component of motion perpendicular to the surface plane, i.e., only those modes which belong to the totally symmetric representation of the point symmetry group of the adsorbate–substrate complex, should couple to the incident EELS beam to produce inelastic scattering via the dipolar mechanism.[6] One might then ask why such a strong loss feature is observed for the ν(CO) mode of η^2-acetone, which for all possible η^2 configurations depicted in Figure 5 is polarized nearly parallel to the surface. First, the highest point group symmetry attainable by each of the possible η^2-acetone configurations is C_s, which results when a mirror symmetry plane exists through the carbon–oxygen bond perpendicular to the surface. In this case, the A_1 ν(CO) mode of free acetone (point group C_{2v}) transforms to the A' representation of the C_s adsorbate complex and is dipolar-active by symmetry considerations alone. Furthermore, the population of the π^*_{CO} orbital of η^2-acetone varies with the carbon–oxygen bond length, causing charge flow to and from the surface as the carbon–oxygen bond vibrates, producing the strong dynamic dipole which leads to the intense inelastic scattering observed for this mode. Comparable effects have been observed for similar parallel modes of C_2H_2 and C_2H_4 [ν(CC)] on Pt(111),[43] $(CH_3)CN$ [ν(CN)] on Pt(111),[44] and O_2 [ν(OO)] on Pt(111),[45] and Ag(110).[46]

No distinction between configurations such as b, c, or d of Figure 5 for η^2-acetone on Ru(001) can be made on the basis of the EELS results. Each would be expected to give methyl and skeletal vibrations similar to those observed and would differ only in the low-frequency vibrations which represent motion of the bonds which coordinate the acetone molecule to the ruthenium surface atoms. These modes are not resolved in the EEL spectra, and no vibrational data in this frequency range for model complexes are available to allow a useful diagnostic comparison. The

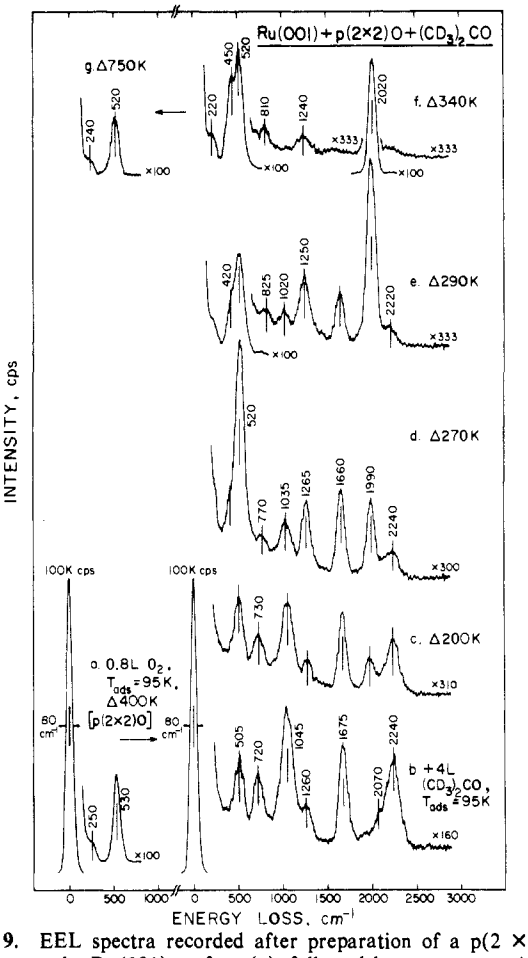

Figure 9. EEL spectra recorded after preparation of a p(2 × 2)O overlayer on the Ru(001) surface (a), followed by exposure to 4 L of $(CD_3)_2CO$ at 95 K, heating to the indicated temperatures, and recooling to 95 K.

details of the η^2-coordination geometry are, of course, far less significant than the fact that η^2 coordination occurs.

Further heating of the Ru(001) surface to 310–315 K results in an attenuation of the features due to η^2-acetone and an increase in the intensities of the features due to adsorbed CO, resulting from decomposition of η^2-acetone (cf. Figure 6d and 7d). Finally, after heating to 340 K, the EEL spectrum of the decomposition products of η^2-$(CH_3)_2CO$, shown in Figure 6e, displays broad, weak bands at 825, 1120, 1370, and 2945 cm^{-1} due to CH_x ($x \leq 3$) hydrocarbon fragments.

D. EELS of Acetone on the Ru(001)–p(2 × 2)O Surface. Exposure of the clean Ru(001) surface to 0.8 L of O_2 at 95 K, followed by annealing to 400 K, produces the EEL spectrum of the p(2 × 2)O overlayer shown in Figure 9a. In addition to the feature at 530 cm^{-1} due to motion of the oxygen adatoms in threefold sites perpendicular to the surface, a mode appears at 250 cm^{-1} which results from coupling of the overlayer to a ruthenium surface phonon.[7] Addition of the p(2 × 2)O overlayer, with an ideal fractional surface coverage of 0.25, changes the work function of the Ru(001) surface by +0.20 eV.[30] When a Ru=O bond length of 2.05 Å[7] is employed and depolarization effects are ignored, this change in work function can be shown[47] to be equivalent to the transfer of 0.02 electron from the ruthenium surface to each oxygen adatom of the p(2 × 2)O overlayer, producing a quantifiable increase in the Lewis acidity of the surface ruthenium atoms.

The effects of the addition of the p(2 × 2)O overlayer on the properties of the acetone adsorbed on the Ru(001) surface are demonstrated dramatically in the EEL spectra of Figures 9 and 10, recorded after exposure of the Ru(001)–p(2 × 2)O surface to 4 L of $(CD_3)_2CO$ and 6 L of $(CH_3)_2CO$ at 95 K, respectively,

(43) Ibach, H.; Hopster, H.; Sexton, B. *Appl. Surface Sci.* **1977**, *1*, 1.
(44) Sexton, B. A.; Avery, N. R. *Surface Sci.* **1983**, *129*, 21.
(45) Gland, J. L.; Sexton, B. A.; Fisher, G. B. *Surface Sci.* **1980**, *95*, 587.
(46) Backx, C.; DeGroot, C. P. M.; Biloen, P. *Surface Sci.* **1981**, *104*, 300.
(47) Topping, J. *Proc. R. Soc. London Ser. A* **1927**, *114*, 67.

Table II. Point Groups and Symmetry Types of Acetone Skeletal Vibrations for Free Acetone and the Adsorbed Configurations Shown in Figure 11

configuration	point group	skeletal mode					
		ν(CO)	ν_s(CCC)	δ(CCC)	ν_a(CCC)	δ(CO)	π(CO)
free	C_{2v}	A_1	A_1	A_1	B_1	B_1	B_2
(a) η^1	C_{2v}	A_1	A_1	A_1	B_1	B_1	B_2
(b) η^1	C_s	A'	A'	A'	A'	A'	A''
(c) η^1	C_s	A'	A'	A'	A''	A''	A'
(d) η^1	C_1	A	A	A	A	A	A
(e) η^2	C_s	A'	A'	A'	A''	A''	A'

followed again by momentary annealing to the indicated temperatures.

The 95 K spectra, Figures 9b and 10a, are dominated by modes due to η^1-acetone and permit rather straightforward assignments (Table I) and interpretation. In the $(CD_3)_2CO$ spectrum, modes at 1675 and 720 cm^{-1} are due to the A_1 ν(CO) and ν_s(CCC) modes of η^1-$(CD_3)_2CO$, while those at 2070 and 2240 cm^{-1} are due primarily to the $\nu(CD_3)$ modes of η^1-$(CD_3)_2CO$ and partly to similar modes of a small amount of η^2-$(CD_3)_2CO$. The feature at 1260 cm^{-1} contains contributions both from the B_1 ν_a(CCC) vibration of η^1-$(CD_3)_2CO$ and the ν(CO) mode of η^2-$(CD_3)_2CO$. The $\delta(CD_3)$ modes from both species are evident at 1045 cm^{-1}, and the broadened band at 505 cm^{-1} results from both the ν(Ru=O) mode of chemisorbed oxygen and the B_1 δ(CO) mode of η^1-$(CD_3)_2CO$. Although the strong $\omega(CH_3)$ and $\nu(CH_3)$ modes in the corresponding $(CH_3)_2CO$ spectrum may indicate the presence of some multilayer or second layer acetone from the slightly larger initial exposure in this spectrum, the observed features can be assigned confidently to η^1-$(CH_3)_2CO$ as follows: $\nu(CH_3)$ at 2995 cm^{-1}, A_1 ν(CO) at 1690 cm^{-1}, $\delta(CH_3)$ at 1440 cm^{-1}, $\omega(CH_3)$ at 1110 and 900 cm^{-1}, and B_1 δ(CO) unresolved from the mode due to adsorbed oxygen at 540 cm^{-1}.

Annealing to progressively higher temperatures attenuates the bands due to η^1-$(CH_3)_2CO$ and η^1-$(CD_3)_2CO$ concomitantly (cf., Figure 9c–e and Figure 10b–d) and reveals bands due to low concentrations of η^2-$(CH_3)_2CO$ and η^2-$(CD_3)_2CO$, the assignments of which parallel those given earlier for the clean surface spectra. The most significant aspect of these annealing sequences is the presence of η^1-acetone at temperatures approaching 300 K, correlating well with the increased stability of molecularly adsorbed acetone at higher temperatures evident in the thermal desorption spectra from the p(2 × 2)O overlayer in comparison to the clean Ru(001) surface. On the clean Ru(001) surface, η^1-acetone was barely detectable by EELS at 200 K, and it was not detected at 275 K. On the Pt(111) surface, η^1-acetone desorbs at 185 K. Consequently, the presence of the p(2 × 2)O overlayer serves to stabilize η^1-acetone compared to η^2-acetone, not only increasing the concentration of the η^1 bonded species, but also increasing its binding energy to the Ru(001) surface, as evidenced by the increased temperature of desorption.

Further heating attenuates the remaining bands due to η^2-acetone as it decomposes. Finally, heating to 750 K retrieves the spectrum of atomic oxygen (cf., Figure 9g), the intensity of which is diminished due to depletion of the oxygen adatoms via reaction with the surface carbon from the decomposition of η^2-acetone.

E. EELS and the Orientations of the Adsorbed Species. The vibrational spectrum of free acetone contains 24 fundamental normal modes, six of which are due to the motion of the C_2CO skeleton, and the remainder of which are due to the internal motion of the methyl groups. The symmetry types of the six skeletal vibrations of free acetone (point group C_{2v}), as well as their frequencies for liquid $(CH_3)_2CO$ and $(CD_3)_2CO$,[39] are listed in Table I.

As was mentioned earlier, the polarizations of the acetone skeletal vibrations (i.e., the orientation of the transition dipole moment of each mode with respect to the symmetry elements of the acetone skeleton) are preserved when acetone is coordinated in an η^1 configuration. For simplicity in the analysis that follows, the surface is assumed to be a structureless flat plane. Inclusion of the effects of the surface structure on the symmetry of the adsorbed species is necessary only when the atoms of the adsorbate

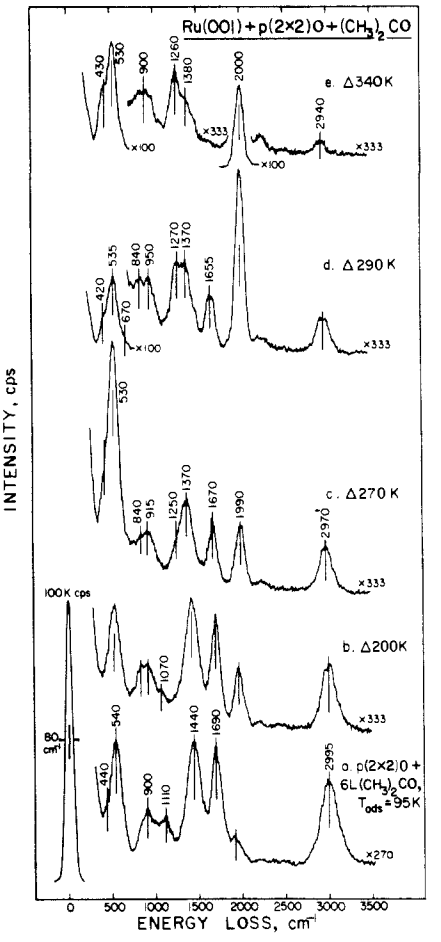

Figure 10. EEL spectra recorded after exposure of the Ru(001)-p(2 × 2)O surface to 6 L of $(CH_3)_2CO$ at 95 K, heating to the indicated temperatures, and recooling to 95 K.

interact strongly with surface atoms other than those to which the adsorbate is coordinated and is therefore superfluous in this analysis for adsorbed acetone. The dipolar activity of each of the acetone skeletal modes as a function of the orientation of the acetone skeleton with respect to the surface plane can be deduced by consideration of the possible coordination geometries shown schematically in Figure 11. The results of this analysis are listed in Table II.

Figure 11a shows the acetone skeleton coordinated to the surface plane in the η^1 configuration of highest possible symmetry (C_{2v}), preserving the C_2 rotational axis and both mirror planes of the free acetone molecule. The A_1 modes of the free acetone skeleton—ν(CO), ν_s(CCC), and δ(CCC)—are polarized parallel to the C_2 axis and strictly perpendicular to the surface plane in this configuration and are therefore dipolar-active. The B_1 modes—ν_a(CCC) and δ(CO)—are polarized in the σ_1 mirror plane strictly parallel to the surface and are dipolar-inactive. The B_2 mode—π(CO)—is polarized in the σ_2 plane, parallel to the surface, and is also dipolar-inactive. Tilting the molecule in the σ_1 plane, as in Figure 11b, reduces the symmetry of the adsorbate complex from C_{2v} to C_s, transforming the A_1 and B_1 modes of C_{2v} to A' of C_s and the B_2 mode to A''. Only the A' modes are dipolar-active.

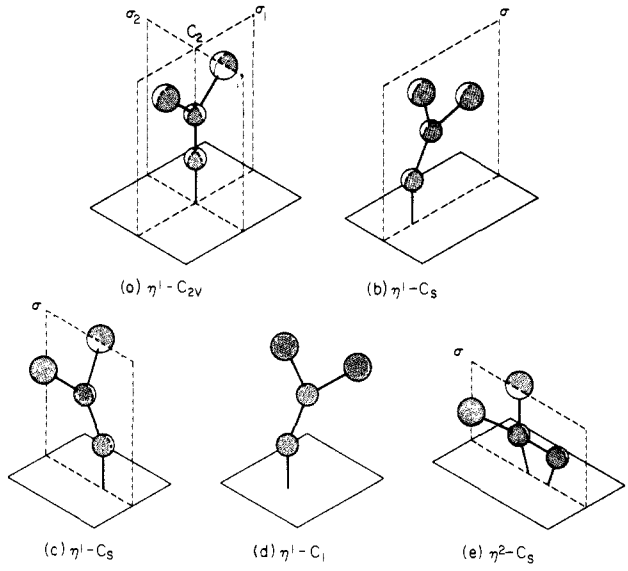

Figure 11. Schematic bonding configurations for η^1-acetone on a structureless flat surface (a–d), illustrating the symmetry elements preserved in each configuration. The η^2 configuration (e) is shown for comparison. In each case, the larger circles represent methyl groups, and the smaller circles represent the carbon and oxygen atoms.

Tilting the molecule in the σ_2 plane produces the C_s configuration shown in Figure 11c, with the A_1 and B_2 modes transforming to A' and the B_1 modes to A''. In Figure 11d, the molecule has been tilted away from both mirror planes, reducing the symmetry to C_1. All modes transform to A of C_1 and are dipolar-active. By the same reasoning as was applied in these examples, an acetone molecule lying flat on the surface could have symmetry no higher than C_s, as is shown for the η^2 configuration in Figure 11e. Note that in terms of symmetry arguments, this configuration is formally equivalent to Figure 11c, and the differences in their vibrational spectra would depend on the effects of the skeletal rehybridization which accompanies the η^2 interaction depicted in Figure 11e.

Returning to the results listed in Table I, obtained from the most clearly resolved spectra of the monolayer η^1 and η^2 species, only modes of A_1 and B_1 symmetry are observed for η^1-acetone on Ru(001), confirming as correct the configuration shown in Figure 11b. This is also the configuration that would be expected to result from the interaction of a single lobe of the oxygen lone pair orbital, a p-type orbital in the plane of the molecule,[48] with a single metal atom of the surface, and agrees with the results obtained for acetone adsorption on Pt(111)[27] and two structurally characterized η^1 complexes of ruthenium, where Ru–O–C bond angles of 153°[11] and 135°[12] have been reported. For the η^2 species, modes derived from the A_1 ν(CO) and ν_s(CCC) and the B_2 π(CO) are observed, confirming e of Figure 11 as the appropriate configuration.

IV. Discussion

The dramatic effect of oxygen preadsorption on the selectivity of the Ru(001) surface toward the nonreactive (η^1) and reactive (η^2) coordination geometries for adsorbed acetone has important implications in the understanding of more complex catalytic reactions. Two possibilities come immediately to mind. The ability to identify and modify selectively those properties of a heterogeneous catalyst which produce the adsorbed intermediate structures which ultimately lead to the desired products could be used to increase the rate and especially the yield for the catalytic reaction. Furthermore, these results may lead directly to a better understanding of how otherwise "inert" coadsorbed species can act as promoters or poisons to affect the product distribution in a heterogeneously catalyzed reaction. To appreciate these possibilities more fully, an understanding of the acetone–ruthenium bonding interaction with and without the effects of coadsorbed oxygen will be developed.

Three factors can be identified which control the type and strength of bonding which coordinate a ligand to a metal center or surface.[22] First, orbitals of the same symmetry must exist on both the ligand and the metal to allow their mixing; second, the spatial extent of the orbitals must be sufficient to facilitate significant overlap; and third, the energies of the interacting orbitals must be similar. Changes in the relative importance of these three factors make one coordination geometry favored over another for a particular ligand–metal system.

Let us first consider the η^1- and η^2-coordination geometries observed for acetone in terms of the "frontier" orbitals of the free acetone ligand.[48] The lowest unfilled orbital is the π^*_{CO}-antibonding orbital, which lies at +4.4 eV with respect to the vacuum level and has its amplitude more strongly localized on the acyl carbon atom than on the oxygen atom. The highest filled molecular orbital is the nonbonding oxygen lone pair, resembling an atomic p-like orbital with lobes localized strongly on the oxygen atom and in the skeletal plane. Its energy lies at 11.2 eV below the vacuum level. The next highest filled level is the π_{CO}-bonding orbital at −12.9 eV, the amplitude of which is slightly greater on the oxygen than on the acyl carbon atom.

An η^1-coordination geometry for organometallic complexes of acetone results from overlap of a single lobe of the nonbonding oxygen lone pair orbital of acetone with a d_σ acceptor orbital of the metal, resulting in a net transfer of electron density from the ligand to the metal. The bent M–O–C bond, identified for the two η^1-acetone complexes of ruthenium mentioned earlier[11,12] and for the orientation of η^1-acetone on both Pt(111)[27] and Ru(001), is a consequence of the spatial distribution of this lone pair donor orbital on acetone. Presumably due to the low amplitude of the π^*_{CO}-antibonding orbital on the oxygen atom, little backdonation from the metal d_π levels to this ligand orbital occurs, as evidenced by the rather small (less than 100 cm^{-1}) red-shifts of the ν(CO) mode observed for homogeneous complexes[9-12] and metal surfaces[27] which bind acetone in this configuration. The role of the metal in this type of interaction is that of a weak Lewis acid, and the purely dative metal–acetone bond which results is correspondingly weak. In many cases, depending on the metal and the properties of other ligands coordinated to it which affect its electronic structure, η^1-acetone complexes are too unstable to be isolated and characterized structurally.[9,10] Thermal desorption results suggest a binding energy of 11.6 kcal/mol for η^1-acetone on the Pt(111) surface,[27] and a similar analysis[49] of the thermal desorption data for Ru(001) suggests binding energies in the range of 10–15 kcal/mol on the clean surface and 10–19 kcal/mol on the Ru(001)-p(2 × 2)O surface.

An η^2-coordination geometry for organometallic complexes of acetone results from overlap of the π_{CO}-bonding orbital of acetone with a d_σ or sp hybrid acceptor level of the metal, along with backdonation from metal d_π levels into the π_{CO}-antibonding orbital of the acetone ligand.[21] The strength of this interaction, and therefore the probability of its occurrence relative to the η^1 interaction, depends critically on the ability of the ligand–metal bond to facilitate backdonation, since in the absence of backdonation the remaining π-donor bond is particularly weak and unstable.[22] Indeed, each of the organometallic complexes isolated and characterized structurally which shows η^2 coordination of ligands similar to acetone[13-20] and the η^2-acetone identified on Ru(001) in this work display substantial rehybridization of the acyl carbon from sp^2 to nearly sp^3, giving clear evidence of efficient backdonation. The fact that backdonation dominates the η^2 interaction has been concluded in similar studies of olefin[50] and acetylene[22,23] bonding to transition metals and illustrates the function of the metal as a Lewis base in these cases.[50] Since transition-metal atoms provide both orbitals of π symmetry to match the symmetry of the π^*_{CO}-antibonding orbital and spatial extent to afford efficient overlap,[22] it is the energy match of the interacting orbitals

(48) Hess, B.; Bruna, P. J.; Buenker, R. J.; Peyerimhoff, S. D. *Chem. Phys.* **1980**, *18*, 267.

(49) Redhead, P. A. *Vacuum* **1962**, *12*, 203.

(50) Ugo, R. *Coord. Chem. Rev.* **1968**, *3*, 319.

which most strongly affects this backbonding interaction.

The effect of d_π and π^*_{CO}-orbital energies on η^2 bonding is illustrated in the properties of the complexes with acetone-like ligands in η^2-coordination geometries. Recall that coordination of acetone to a number of transition metals, including rhodium and iridium[10] and ruthenium,[11,12] produces η^1 complexes. Substitution of hydrogen for CH_3 in acetone, however, lowers the energy of the π^*_{CO}-antibonding orbital from +4.4 to +3.1 eV,[48] decreasing the energy gap between the π^*_{CO} and d_π levels. This enhances d_π to π^*_{CO} backdonation, and η^2-formaldehyde complexes with a number of metals, including osmium[13] and iron,[14] result. Substitution of the more electronegative CF_3 for CH_3 depolarizes the carbon–oxygen bond of hexafluoroacetone relative to acetone, lowering its π^*_{CO}-orbital energy dramatically and yielding η^2 complexes with electronegative metals such as platinum[15,19] and nickel.[16,17] Of particular significance with respect to these arguments is that the only unsubstituted η^2-acetone complex isolated to date is formed with a low valent and electropositive tantalum center.[18] The lower d-level occupancy of tantalum ($5d^36s^2$) relative to rhodium ($4d^85s^1$), iridium ($5d^76s^2$), and ruthenium ($4d^75s^1$) ensures that its d levels have higher energy and therefore can more easily populate the π^*_{CO} level of acetone to facilitate η^2 bonding.

On the basis of these arguments, the formation of η^2-acetone on the Ru(001) surface can be understood. Interactions among metal atoms at a surface broaden the d levels to form bands which extend to higher energies than the d levels of isolated metal atoms (i.e., the Fermi level of a bulk metal is at a higher energy than the highest occupied level of an isolated metal center),[51] causing the atoms of the surface to behave as isolated metal atoms of lower net d-level occupancy. In effect, metal atoms at a surface are more electron rich than isolated atoms in a complex and can therefore raise their formal oxidation state more easily to yield backdonor bonding. The π^*_{CO} orbital of acetone is apparently at the appropriate energy to allow a dramatic distinction between the behavior of the Ru(001) surface, where the Fermi level is at −5.4 eV[52] and where substantial η^2 bonding of acetone occurs, and the Pt(111) surface, the increased d-level occupancy of which ($5d^96s^1$) lowers its Fermi level to −5.9 eV[53] and thus favors η^1 bonding.

It remains to explain in these same terms the effect of coadsorbed oxygen on the bonding of acetone on Ru(001). As was discussed previously, the p(2 × 2)O overlayer increases substantially both the concentration and the stability of η^1-acetone on the Ru(001) surface. We attribute this to a "short-range" through-metal electron deficiency at neighboring ruthenium surface sites, due to the presence of the electronegative oxygen adatoms, increasing the Lewis acidity of the former. The stability of other surface species coordinated to the Ru(001) surface via σ-donor bonds shows a similar enhancement in the presence of coadsorbed oxygen, including N_2,[54] N_2O,[55] and bridge-bonded formate.[56]

Addition of the p(2 × 2)O overlayer increases the work function of the Ru(001) surface by 0.20 eV (i.e., lowers the Fermi level by 0.20 to −5.6 eV),[30] increasing the disparity between the energy of the occupied d band of the metal and that of the π^*_{CO} acceptor level of acetone. This renders backdonation more difficult and causes Ru(001) to behave more like Pt(111). The implications of this for the effects of catalyst poisons and promoters are interesting: adsorption of electronegative substituents such as sulfur would produce an increase in the surface work function similar to oxygen and should therefore inhibit reactions which proceed through backbonded intermediates, whereas the adsorption of "cationic" species such as potassium would decrease the surface work function and should promote the formation of backbonded intermediates (based solely on the shift in energy difference between the donor and acceptor levels caused by each). The net effects of these bonding interactions on the surface chemistry of acetone adsorbed on both the clean Ru(001) and the Ru(001)–p(2 × 2)O surfaces may be illustrated by overall reaction schemes for the monolayer species adsorbed on both surfaces, which result from consideration of both the EELS and thermal desorption results discussed previously.

On the clean Ru(001) surface, both η^1- and η^2-acetone are produced upon adsorption of a saturated first layer of acetone at 95 K

$$(CH_3)_2CO(g) \rightarrow \eta^1\text{-}(CH_3)_2CO$$

and

$$(CH_3)_2CO(g) \rightarrow \eta^2\text{-}(CH_3)_2CO$$

Heating the surface causes η^1-acetone to desorb molecularly in the temperature range between approximately 150 and 250 K,

$$\eta^1\text{-}(CH_3)_2CO \rightarrow (CH_3)_2CO(g)$$

whereas η^2-acetone decomposes between approximately 200 and 320 K to adsorbed CO and CH_3 fragments:

$$\eta^2\text{-}(CH_3)_2CO \rightarrow CO(a) + 2CH_3(a)$$

Decomposition of the CH_3 fragments follows rapidly through CH_x ($x < 3$) intermediates

$$CH_3(a) \rightarrow CH_2(a) + H(a) \rightarrow CH(a) + 2H(a) \rightarrow C(a) + 3H(a)$$

Adsorbed CO is evolved from the surface in a desorption rate-limited reaction near 470 K,

$$CO(a) \rightarrow CO(g)$$

and hydrogen adatoms from CH_x decomposition recombine on the surface to evolve H_2 in a desorption rate-limited reaction near 330 K and a series of reactions between 400 and 750 K which have their desorption rates limited by the rates of decomposition of the CH_x fragments on the surface in this temperature range:

$$2H(a) \rightarrow H_2(g)$$

Adsorbed carbon from the methyl groups remains on the surface. The total amount of CO and H_2 evolution from the surface indicates that approximately one-eighth of the monolayer of η^2-acetone adsorbs and decomposes on the clean Ru(001) surface under these conditions.

On the Ru(001)–p(2 × 2)^{18}O surface, substantially more η^1-acetone and less η^2-acetone are formed upon adsorption at 95 K compared to the clean surface. Heating of the surface causes η^1-acetone to desorb molecularly in the temperature range between approximately 150 and 320 K, and the remaining η^2-acetone decomposes to adsorbed CO and CH_3 fragments in the temperature range between 200 and 350 K. The p(2 × 2) oxygen overlayer not only increases the yield of η^1-acetone and stabilizes it to higher desorption temperatures, but it also retards the rate of decomposition of η^2-acetone, as evidenced by its persistence in EEL spectra of higher temperatures on the Ru(001)–p(2 × 2)O surface than on the clean surface. Decomposition of the CH_3 fragments follows rapidly after their formation, producing H_2 in desorption rate-limited reactions near 220 K and a series of reactions between 250 and 550 K, the desorption rates of which are limited by the rates of decomposition of the adsorbed CH_x fragments. The CO produced from the decomposition of η^2-acetone (m = 28 amu) is evolved in a desorption rate-limited reaction at 450 K, and C^{18}O produced by the reaction of adsorbed carbon from CH_3 decomposition with the oxygen adatoms (^{18}O) of the p(2 × 2) overlayer (m = 30 amu) is evolved between 400 and 700 K. The total amounts of CO (m = 28 amu), H_2, and C^{18}O (m = 30 amu) evolution from the surface indicate that

(51) Saillard, J.-Y.; Hoffmann, R. *J. Am. Chem. Soc.* **1984**, *106*, 2006.
(52) Himpsel, F. J.; Christmann, K.; Heinmann, P.; Eastman, D. E. *Phys. Rev. B* **1981**, *23*, 2546.
(53) Nieuwenhuys, B. E.; Sachtler, W. H. M. *Surface Sci.* **1973**, *34*, 317.
(54) Anton, A. B.; Avery, N. R.; Madey, T. E.; Weinberg, W. H., in preparation.
(55) Madey, T. E.; Anton, A. B.; Avery, N. R.; Weinberg, W. H., in preparation.
(56) Toby, B. H.; Avery, N. R.; Anton, A. B.; Weinberg, W. H., in preparation.

approximately 0.02 monolayer of η^2-acetone adsorbs and decomposes on the Ru(001)-p(2 × 2)O surface under these conditions.

Two pathways can be postulated for the decomposition of η^2-acetone on the Ru(001) surface. In one case, the acetone skeleton would decompose initially through C–C bond cleavage to produce CO and methyl groups on the surface. Since molecular dissociation in general proceeds through population of an antibonding molecular orbital,[51,57] the difference in reactivity of the Ru(001) surface toward η^1- and η^2-acetone would be a clear and obvious manifestation of the bonding interactions which lead to the formation of each species if C–C bond cleavage were the dominant dissociation channel. The reaction coordinate for this mechanism would be the ν(CO) vibration of η^2-acetone, since its amplitude controls most directly the population of the π^*_{CO}-antibonding orbital, and this orbital in turn controls the integrity of the acetone skeleton. A second possible mechanism invokes first C–H bond cleavage, with decomposition of the destabilized acetone skeleton following rapidly thereafter. In this case, η^2-acetone, with its methyl groups in closer proximity to the ruthenium surface atoms than the η^1 species, would again be expected to be more reactive. Decomposition would proceed via population of the $\pi^*_{CH_3}$-anitbonding orbital of acetone, and either the π(CO) vibration of η^2-acetone near 600 cm^{-1}, the motion of which controls the approach of the methyl groups to the surface, or the ν(CH) vibration would represent the reaction coordinate. A distinction between these possibilities could only be made if the experimental results showed clear evidence of a kinetic isotope effect. For example, if the decomposition of η^2-$(CD_3)_2CO$ occurred at higher temperatures than η^2-$(CH_3)_2CO$, this would identify ν(CH) as the reaction coordinate and C–H bond cleavage as the rate-limiting step in η^2-acetone decomposition. Such a kinetic isotope effect was not observed, however. Since the π^*_{CO} orbital of acetone is already partially populated in the stable η^2 configuration, and since the $\pi^*_{CH_3}$ orbital is at significantly higher energy than the π^*_{CO} orbital (16.5 vs. 8.2 eV for free acetone[48]), decomposition of η^2-acetone via C–C bond cleavage would appear to be the favored mechanism.

(57) Sung, S.-S.; Hoffmann, R. *J. Am. Chem. Soc.* **1985**, *107*, 578.

V. Summary

The important conclusions of this work may be summarized as follows:

(1) Acetone bonds molecularly to the Ru(001) surface at 95 K in two different configurations: an η^1 (end-on) configuration which desorbs reversibly and an η^2 (side-on) configuration which dissociates upon heating of the surface.

(2) The η^2 configuration is the majority species on the clean Ru(001) surface. The appearance of a red-shifted ν(CO) vibration near 1300 cm^{-1} indicates significant rehybridization of the acyl carbon in this configuration, to that found for homogeneous organometallic complexes with η^2-ketonic ligands.

(3) The η^1 configuration is adsorbed with C_s symmetry and a nonlinear Ru–O–C bond, as has been observed in analogous organometallic η^1 complexes of acetone.

(4) Addition of an ordered p(2 × 2) overlayer of oxygen adatoms to the Ru(001) surface stabilizes the η^1 configuration of adsorbed acetone, rendering it the majority surface species and increasing its binding energy relative to the clean surface.

(5) The selectivity of the Ru(001) and the Ru(001)-p(2 × 2)O surfaces toward the η^1- and η^2-acetone bonding configurations can be explained in terms of the electronic properties of these surfaces and their effects on the bonding interactions which dictate the two coordination geometries.

Acknowledgment. We thank Profs. R. H. Grubbs and J. E. Bercaw for valuable discussions during the preparation of this manuscript. This research was supported by the National Science Foundation under Grant CHE82-06487.